SEPARATIONS

New Methodology for the Measurement and Analysis of Adsorption Dynamics: Butane on Activated Carbon

Shaheen A. Al-Muhtaseb*,† and James A. Ritter‡

Department of Chemical and Petroleum Engineering, College of Engineering, UAE University, P.O. Box 17555, Al-Ain, United Arab Emirates (UAE), and Department of Chemical Engineering, Swearingen Engineering Center, University of South Carolina, Columbia, South Carolina 29208

The dynamic uptakes of *n*-butane on Westvaco BAX-1100 activated carbon were measured over the temperature and pressure ranges of 283−383 K and ∼3−1000 Torr, respectively. The experimental uptakes were used to determine the overall linear driving force (LDF) mass-transfer coefficients and their statistically significant dependences on the operating conditions (temperature and loading). Moreover, the effects of temperature on the order of the parabolic concentration profiles inside the adsorbent particle were determined, and the role of these effects in providing the proper description of the energy-activated mechanism of diffusion was established over the studied range of operating conditions. Overall, it was indicated that the energy barrier for diffusion is independent of temperature and that it increases with increasing adsorbent surface coverage with the adsorbate. Nevertheless, a transient state of diffusion was indicated in which an apparent energy barrier for diffusion appears to depend on temperature.

1. Introduction

The simulation of cyclic adsorption processes for the separation of gas components that have a dynamic-controlled character of adsorption from mixtures depends strongly on the accurate description of the mass-transfer properties. This dependence becomes more critical in the modeling of transient (unsteady-state) adsorption processes and under extreme operating conditions when the equilibrium-controlled character of adsorption becomes subordinate. To further complicate matters, the dominating mechanism of diffusion can be very complex and can vary with the process operating conditions.[1,2] The most commonly encountered diffusion mechanisms in adsorption processes are molecular (pore), Knudsen, and surface diffusions, as well as Poiseuille (viscous) flow. Nonetheless, the effects of molecular (pore) diffusion and Poiseuille flow, both being dominant in large pores and at relatively high pressures,[2] are usually negligible in highly porous adsorbents where the dominant diffusion mechanism tends to be surface diffusion.[3−5] A detailed description of these mechanisms and the range of operating conditions under which they dominate is given in the literature.[1,2] Moreover, surface diffusion, which is again considered to be one of the most important mass-transfer mechanisms in adsorption processes,[3−5] is an energy-activated mechanism,[6,7] and it has been shown to be largely dependent on the operating conditions (temperature and fractional surface coverage or pressure).[4,8−15] Overall, these different modes of diffusion can be estimated with various experimental approaches, such as the measurement of dynamic uptake curves,[16] which is the focus of this work.

The linear driving force (LDF) approximation, which represents a parabolic concentration profile of the adsorbed species within a spherical adsorbent particle,[17,18] is sufficient to describe the overall dynamic uptake on heterogeneous adsorbents, as well as adsorption-column breakthrough behavior.[19] However, the validity of the LDF approximation is limited to time scales above ∼1 or 100 s for activated carbons and zeolite crystals, respectively.[20] This limitation could be improved by incorporating a time dependence of the mass-transfer coefficient into the LDF equation.[21−23] Although the LDF model is originally based on linear adsorption isotherms,[24] it has been shown that nonlinear adsorption isotherms can also yield a similar form under certain conditions.[25−27] The general treatment of the LDF model needs to consider the effects of nonlinear isotherms to avoid erroneous analyses.[28]

Overall, it has been shown that the proper description of the dynamic, nonequilibrium adsorption uptake curves and its dependence on the operating conditions are essential for the complete description of the approach to equilibrium within a single adsorbent particle.[25,26] However, there is a paucity of published literature that examines the roles of these effects on the accurate prediction of cyclic adsorption process behavior, despite the popularity of the LDF model in modeling cyclic adsorption processes.[29] Therefore, this work was carried out as a further investigation of a previous effort[30] and aims to establish an experimental and mathematical protocol for the determination and investigation of the mass-transfer characteristics of, for

* To whom correspondence should be addressed. E-mail: s.almuhtaseb@uaeu.ac.ae. Tel.: (971-3) 7051-545. Fax: (971-3) 7624-262.

† UAE University.

‡ University of South Carolina.

10.1021/ie049629r CCC: $27.50
Published on Web 09/22/2004

example, the adsorption of *n*-butane on BAX-1100 activated carbon.

Rather than trying to provide direct mechanistic insight into this adsorbate−adsorbent system, the goal of this work is to provide a systematic protocol for determining the temperature and loading dependence of the mass-transfer coefficient that could subsequently be used in pressure swing adsorption (PSA) process simulations to more accurately predict the dynamic process behavior as shown in the previous study.[30] For this reason, broader ranges of temperature and pressure, along with a more comprehensive analysis of the roles of the thermal and operating conditions in the estimated mass-transfer properties, are addressed here. The experiments were also carried out over very small pressure steps to eliminate the effects of adsorption isotherm nonlinearities and any potential dependence of the diffusion coefficients on the average concentration. Moreover, the short-time correction of the LDF model is addressed in this work through the adoption of a dynamic concentration parabolic profile that flattens gradually with time.

2. Theory

Dynamic, nonequilibrium adsorption uptakes describe the variation of the amount adsorbed of a specific component with time. The fractional uptake is expressed with different models such as the LDF approximation, which results in the following expression

$$\frac{m_t}{m_\infty} = 1 - \exp[-3(n+3)kt] \qquad (1)$$

where m_t and m_∞ are the instantaneous and equilibrium amounts adsorbed, respectively; t is the time; and k is the overall mass-transfer coefficient. n represents the polynomial degree of the parabolic concentration profile of the adsorbed component inside the adsorbent particle. Equation 1 can be used with a constant value of n (e.g., $n = 2$) or with a time-decaying exponential form such as

$$n = n_0 \exp(n_1 t) \qquad (2)$$

where n_1 is negative.

The overall mass-transfer coefficient is one of the most important parameters for simulating cyclic adsorption processes, such as PSA, because it indicates the rate of variation of the amount adsorbed with time. This rate is given with the LDF approximation by

$$\frac{\partial q_i}{\partial t} = 3(n+3)k_i(q_i^* - q_i), \quad i = 1, 2, ..., N \qquad (3)$$

where q is the instantaneous amount adsorbed per unit mass of adsorbent, i is an indicator for different species in the mixture, N is the number of species, and the asterisk denotes the equilibrium amount adsorbed. Equation 3 constitutes one of the most important relationships in the component, total mass, and energy balances that mathematically describe the PSA process.[31]

3. Experimental Section

The nonequilibrium dynamic uptake curves for the adsorption of CP-grade *n*-butane (C_4) (used as received from National Welders) on 23.7 mg of MeadWestvaco BAX-1100 activated carbon were measured gravimetrically using a VTI microbalance (located at the University of South Carolina) with LabView software developed in-house. The BAX-1100 activated carbon was obtained from MeadWestvaco in the form of pellets (2.1 mm extruded) and used as received, except for regeneration. Prior to each isotherm measurement, the activated carbon was regenerated at 523 K for 2 h under a vacuum of less than 1×10^{-5} Torr.

The dynamic uptakes of C_4 were measured at 10, 15, 25, 35, 50, 75, and 110 °C and were generated by introducing uniform pressure step changes of ∼3 Torr in the range from ∼3 to ∼97 Torr and monitoring the variations of the weight of the sample versus time.[30] The time resolution between each pair of successive points was on the order of 0.14 s, and the precisions of the weight and temperature measurements were 1 μg and 0.1 K, respectively. Pressure step changes were chosen to be of this magnitude (∼3 Torr) to minimize exother-

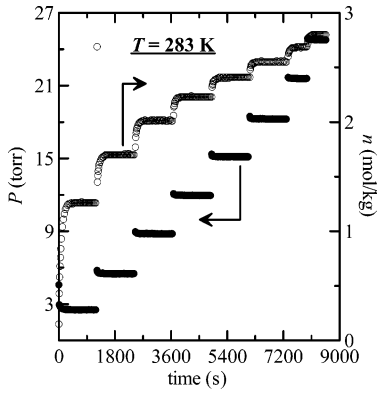

Figure 1. Sample input pressure steps and the corresponding loading output measurements (solid and empty symbols, respectively) at 283 K. Number of data points plotted was reduced for clarity.

Table 1. Average and Equilibrium Amounts Adsorbed (mol/kg) as a Function of Pressure (Torr) and Temperature (K) with the Three-Process Langmuir and Logarithmic Isotherm Correlations

	amount adsorbed	
	average	equilibrium
Three-Process Langmuir Correlation[a]		
m_1 (mol/kg)	7.302 163 9	7.062 063 9
b_{01} (Torr^{-1})	7.152×10^{-9}	1.271×10^{-9}
b_{11} (K)	3561.7707	4113.2139
m_2 (mol/kg)	0.039 538 3	2.703 661 6
b_{02} (Torr^{-1})	0.999 607 7	4.08×10^{-7}
b_{12} (K)	3432.1514	3708.6487
m_3 (mol/kg)	2.680 545 1	0
b_{03} (Torr^{-1})	5.307×10^{-7}	0
b_{13} (K)	3564.0995	0
ARE (%)	15.53	8.43
Logarithmic Isotherm Correlation[b]		
$A_{0,0}$	54.0543	51.350 23
$A_{0,1}$	−9.738 44	−9.124 73
$A_{1,0}$	−9.378 44	−8.422 11
$A_{1,1}$	1.781 379	1.561 721
$A_{2,0}$	0.716 203	0.612 686
$A2,1$	−0.133 45	−0.110 45
ARE (%)	16.30	8.34

[a] Three-process Langmuir correlation:

$$q = \Sigma_{j=1}^{3} m_j \frac{b_{0j} \exp(b_{1j}/T)P}{1 + b_{0j} \exp(b_{1j}/T)P}$$

[b] Logarithmic correlation:

$$q = \exp(\Sigma_{j=0}^{2}[(A_{j,0} + A_{j,1} \ln T)(\ln P)^j])$$

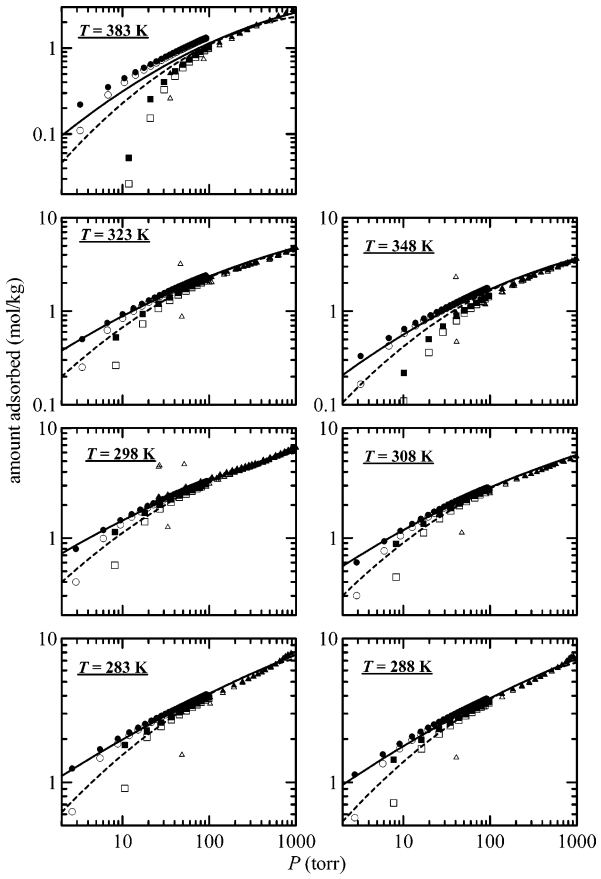

Figure 2. Equilibrium and average amounts adsorbed (filled and empty symbols, respectively) over the pressure ranges of 0−1000 Torr (△) and 0−100 Torr with steps of ∼3 (○) and 10 Torr (□). Solid and dashed lines represent the logarithmic isotherm correlation.

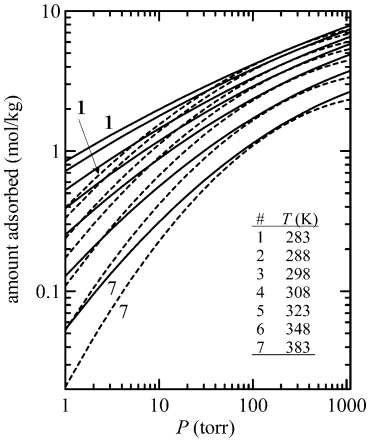

Figure 3. Temperature dependences of the equilibrium and average amounts adsorbed (solid and dashed lines, respectively) obtained from the logarithmic isotherm correlation over the whole range of 0−1000 Torr.

mic heat effects while maintaining resolution of the measured dynamic uptakes over the total range of pressure. Figure 1 shows a sample of the induced pressure steps and the resulting increases in the amount adsorbed of C_4 versus time. To investigate the role of the heat of adsorption on the estimated mass-transfer coefficients, the same procedure was repeated with pressure steps of ∼10 Torr in the range from ∼10 to ∼100 Torr. These measurements were complemented by scaling up the pressure range to ∼30 to ∼1000 Torr in steps of ∼30−100 Torr.

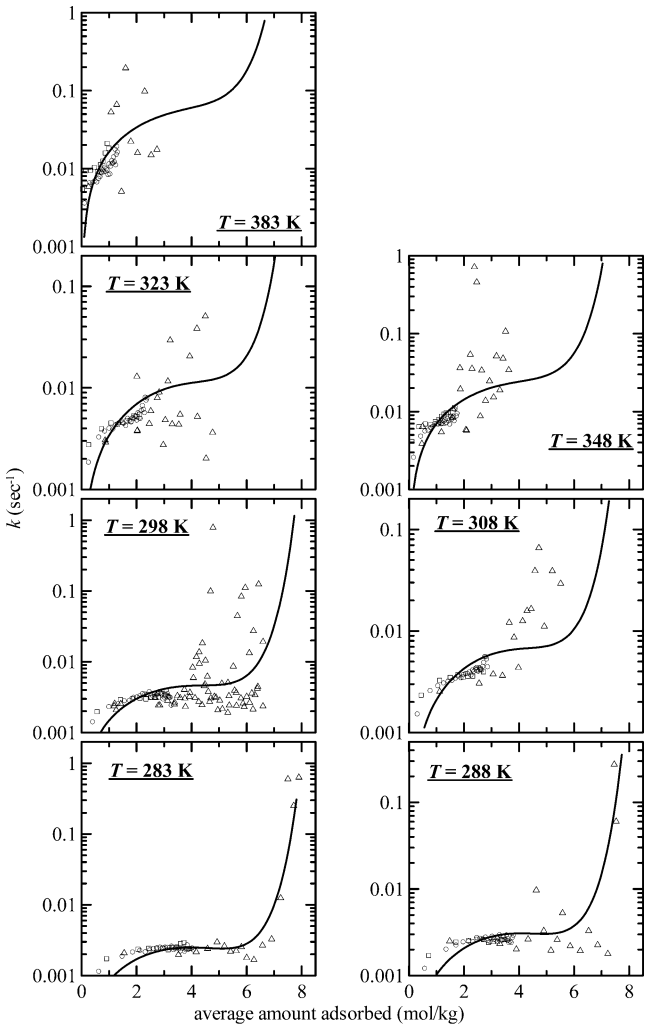

Figure 4. Optimized (symbols) and correlated (lines) time-independent LDF mass-transfer coefficients over the pressure ranges of 0−1000 Torr (△) and 0−100 Torr with steps of ∼3 (○) and 10 Torr (□).

4. Results and Discussion

To characterize the fractional uptake experiments in terms of loading instead of pressure, the equilibrium amounts adsorbed were estimated from the average weights of the sample taken over ∼2−3 s after reaching equilibrium. Overall, ∼2−5 min was required for each uptake to reach equilibrium. The average amount adsorbed for each pressure step was defined by the mean of the equilibrium amounts adsorbed before and after the pressure step. Table 1 shows the expressions and fitted parameters for three-process Langmuir and logarithmic-type correlations for the equilibrium and average amounts adsorbed. The model parameters were obtained by minimizing the sum of squared errors (SSE) of q and $\ln q$, respectively; the resulting average relative errors (AREs) in the correlated amount adsorbed are also reported in Table 1. Given that the logarithmic-type correlation was more concise and accurate than the three-process Langmuir correlation, it was considered to be more descriptive of the experimental results. Figure 2 shows a contrast between the logarithmic-type correlation and the equilibrium and average amounts adsorbed, and Figure 3 shows the difference between the average and equilibrium amounts adsorbed over the entire range of temperatures. It is clear from Figures 2 and 3 that the deviation between the average and

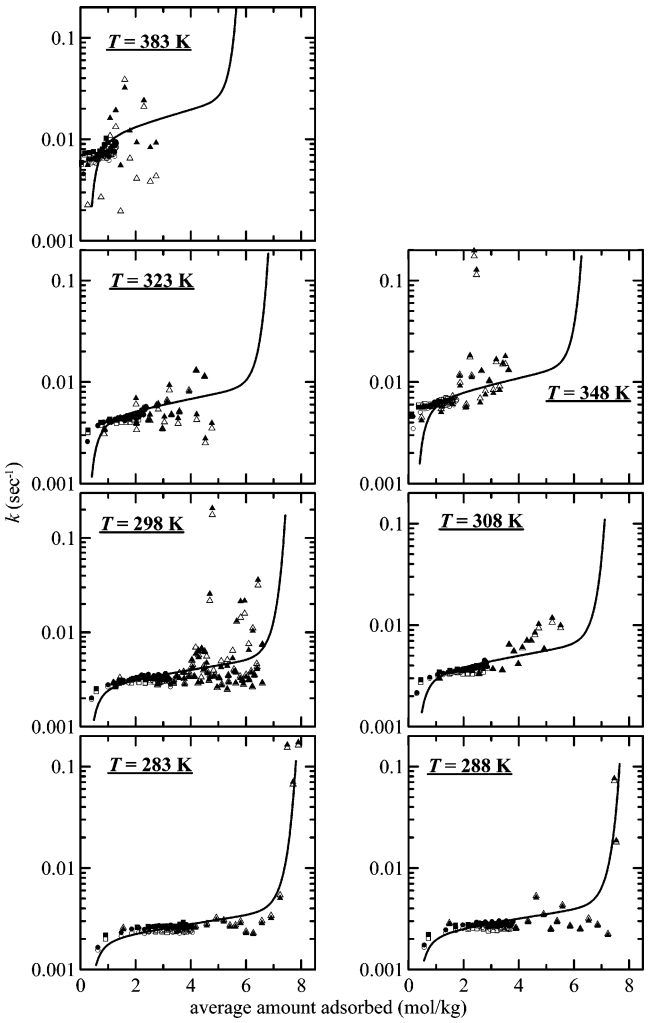

Figure 5. Optimized (symbols) and correlated (lines) time-dependent LDF mass-transfer coefficients over the pressure ranges of 0−1000 Torr (△) and 0−100 Torr with steps of ∼3 (○) and 10 Torr (□). Filled and empty symbols denote mass-transfer coefficients optimized with raw and correlated degrees of parabolic concentration profiles, respectively, and the correlations (lines) correspond to the latter case.

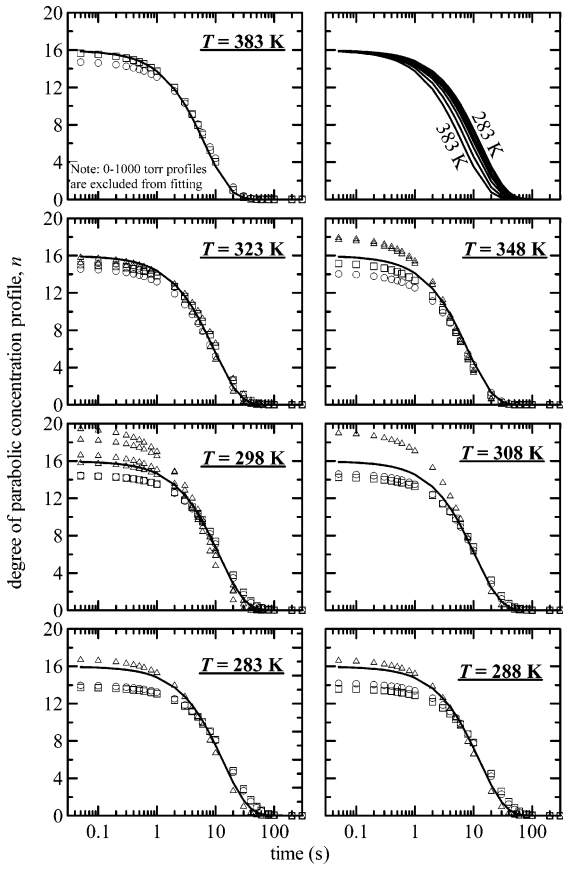

Figure 6. Variation of degree of parabolic concentration profiles with time over the pressure ranges of 0−1000 Torr (△) and 0−100 Torr with steps of ∼3 (○) and 10 Torr (□). The correlated temperature effect on the degree of the parabolic concentration profiles is summarized in the upper right subplot.

Table 2. List of 107 Predictors Allowed to Compete Statistically for the Significant Description of ln(k)[a]

1	$(qT)^{0.5}$	$\exp(T)$	$\ln(q^{\pm1})$
$T^{\pm m}$	$(q^{-1})^{0.5}$	$\exp(T^{-m})$	$\ln(q^{\pm2})$
$q^{\pm j}$	$(q^{-1}T^{\pm1})^{0.5}$	$\exp(q^{-j}T)$	$\ln(T^{\pm1})$
$q^{\pm j}T^{\pm m}$	$\exp(q^{\pm j})$	$\exp(q^{\pm j}T^{-m})$	$\ln[(q^{-1})^{0.5}]$
$q^{0.5}$	$\exp(q^{\pm0.5})$	$\exp[(q^{\pm1}T^{\pm1})^{0.5}]$	$\ln[(q^{\pm1}T^{\pm1})^{0.5}]$
$(qT^{-1})^{0.5}$			

[a] Stepwise regression criteria: $P_{IN} = 5\%$ and $P_{OUT} = 10\%$; j and m = 1, 2, or 3.

equilibrium amounts adsorbed becomes most significant at very low temperatures or amounts adsorbed. Therefore, the distinction between the two amounts adsorbed in describing the uptake process is most important under such conditions.

Each of the uptakes measured as described above was fitted individually by minimizing the SSE in correlating the fractional uptake according to eq 1 with both an exponentially time-decaying n value and a constant n value of 2. The optimized k values with $n = 2$ and $n = n(t,T)$ are shown in Figures 4 and 5, respectively (symbols). It is clear from both cases that the differences between the optimized k values obtained with different pressure step sizes are minimal. Therefore, because the pressure step size is one of the direct factors that determine the magnitude of heat evolution due to adsorption, this indicates that the optimum k values are practically independent of the amount of heat evolved during the uptake step. Moreover, except for minor scattering, it is clear from Figures 4 and 5 that the optimum k values follow an almost fixed trend versus the average amount adsorbed and temperature. However, the k values optimized with the time-dependent concentration profiles resulted in less scattering than those with constant n. Along with k values for time-dependent concentration profiles, n was fitted for each temperature and assumed to be fixed throughout the consecutive pressure steps within the same experiment. Figure 6 shows the optimized n values versus time, where the magnitudes of the pressure steps show no effect on the optimum values. However, it seems that the magnitude of the total pressure has a minor effect on n, as evident by the frequent deviations between the n values over the ranges of ∼30−1000 and ∼3−97 Torr with different step sizes. Overall, it seems that the intercept of n at $t = 0$ (or n_0) is almost constant and that only the degree of the exponential decay (n_1) depends on temperature. Therefore, the optimum n values were fitted satisfactorily according to eq 2 with the following correlation

$$n(t,T) = 15.977 \exp[(0.1392 - 7.576 \times 10^{-4}T)t] \quad (4)$$

It is clear from eq 4 that the steepness of the concentra-

Table 3. SW Regression Results for the Overall Mass-Transfer Coefficients with Fixed and Variable Degrees of Parabolic Concentration Profiles

	k ($n = 2$)			k [$n = n(t)$]		
i	c_i	v_i	τ_i	c_i	v_i	τ_i
1	−2859.265	T^{-1}	−19.603	−1768.517	T^{-1}	−72.046
2	2.159	$\ln[(Tq)^{0.5}]$	9.563	1.256×10^{-20}	$\exp[(Tq)^{0.5}]$	12.596
3	6.974×10^{-3}	$\exp(q)$	6.817	1.190×10^{-6}	T^2q	5.169
4	−3.084	$\exp(q^3T^{-1})$	−5.492	-6.810×10^{-4}	Tq^{-2}	−2.944
ARE (%)		10.35			5.08	

tion profile increases with increasing temperature. Behaviors correlated according to eq 4 are plotted in Figure 6 against the optimized data, and the collective variation with temperature is shown in the upper right corner of Figure 6.

To obtain the best correlations for the variation of k with temperature and average amount adsorbed, $\ln(k)$ was subjected to stepwise (SW) regression (as described elsewhere[32]) versus a collection of combinations of the independent variables T and q, where q is the average amount adsorbed. The proposed formula for the SW regression was

$$\ln k = \sum_i c_i v_i \tag{5}$$

where v_i is each combination of the independent variables and c_i is the coefficient (constant) of this combination. A list of the combinations allowed to compete for the statistical description of $\ln(k)$ is given in Table 2. The SW regression procedure compares the changes in the statistical significance of the correlated variable after the entry and removal of each of those variables. With input and removal criteria of probabilities of 5% and 10%, respectively, only four of the 107 predictors listed in Table 2 survived this SW regression and proved to be statistically significant in describing $\ln(k)$ in each case. The results from the SW regression, with n either fixed at 2 or given by eq 4, are reported in Table 3, along with the average relative errors (AREs) in correlating the experimental fractional uptakes and the significance indicator (τ) for each term. Knowing that higher absolute values of τ denote higher significances in describing the dependent variable, it becomes clear that the most dominant descriptor of $\ln(k)$ is $1/T$, which represents an Arrhenius behavior. Therefore, it is believed that the diffusion process is mostly dominated by an energy-activated mechanism such as surface diffusion. The two correlations shown in Table 3 are contrasted with the optimized data in Figures 4 and 5 for constant and time-dependent n, respectively.

Figure 7 shows a comparison between the k values with constant and time-dependent n's. It can be seen that the two approaches give almost equivalent values, especially at moderate temperatures or at low temperatures and high loadings. Therefore, it can be judged that k (which also represents the overall mass-transfer, or diffusion, coefficient) is dependent mostly on the operating conditions (T and q) and to a much lesser extent on the concentration profile inside the particle of the adsorbent. Moreover, Figure 7 shows the expected behavior of increasing the overall mass-transfer coefficient when increasing the temperature, as expected because of the increase of the kinetic energy of the adsorbed molecules with temperature. This behavior might reflect the importance of a Knudsen diffusion mechanism also contributing to the surface diffusion flux. Nevertheless, the increase of the mass-transfer coefficient with loading was most significant at very low and very high loadings. These two regions correspond first to a clean adsorbent surface, which has a marked affinity for adsorbing molecules, and second to a highly covered surface, which is characterized by an increase in the surface diffusion possibly due to the well-accepted hopping kind of mechanism associated with crowed surfaces.[2] Nevertheless, moderate loadings (i.e., $q = \sim 1-6$ mol/kg) exhibit negligible effects on the overall mass-transfer coefficient.

Figure 8 shows the Arrhenius plots for the k values correlated with constant and time-dependent concentration profiles. Clearly, the k values correlated with the constant n always exhibited an Arrhenius-type behav-

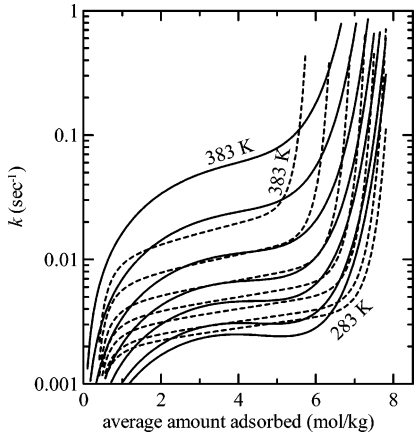

Figure 7. Overall temperature and loading effects on the LDF mass-transfer coefficients optimized with second-order and time-dependent degrees of the parabolic concentration profiles (solid and dashed lines, respectively).

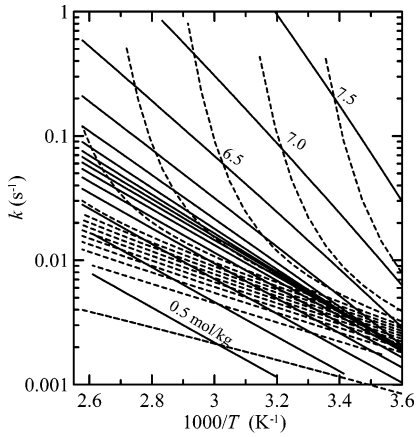

Figure 8. Arrhenius plots of temperature and loading effects on the LDF mass-transfer coefficients optimized with second-order and time-dependent degrees of the parabolic concentration profiles (solid and dashed lines, respectively).

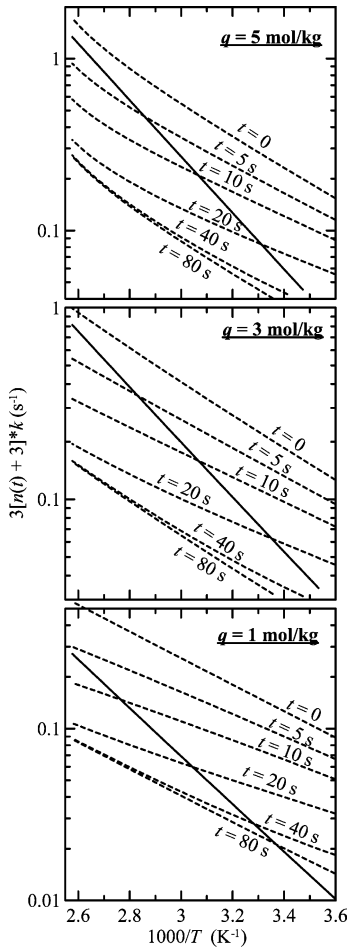

Figure 9. Arrhenius plots of temperature and loading effects on the LDF mass-transfer coefficients optimized with second-order and time-dependent degrees of the parabolic concentration profiles (solid and dashed lines, respectively) multiplied by 3(n + 3).

ior, but with an increasing slope with loading. The variations of these slopes can be used as indicators of the magnitude of the activation energy for diffusion under different operating conditions. On the other hand, k values with time-dependent n deviated from the Arrhenius (linear) behavior, especially at high loadings. Moreover, the k values correlated with the time-dependent n exhibited infinite values at high loadings and high temperatures (low 1/T). Nevertheless, accounting for the temperature dependence of n (correlated in eq 4) as an essential part of the overall mass-transfer coefficients, i.e.

$$k' = 3[n(t,T) + 3]k \qquad (6)$$

recovers the expected Arrhenius (linear) behavior of k' calculated with the time-dependent n as shown in Figure 9. Figure 9 also shows that k' values calculated with $n = 2$ are generally equivalent to those calculated with a time-dependent n under moderate conditions and specifically at short times and high temperatures or at long times and low temperatures. Moreover, Figure 9 shows that the time effects on k' is most significant at short times, which is equivalent to the behavior indicated from n in eq 4. Nevertheless, the effects of time on the slope are mostly negligible.

This characteristic Arrhenius behavior of k' gives rise to the determination of the slope of the linear functions, which can be used as an indicator of the magnitude of the activation energy barrier for the energy-activated diffusion mechanisms. Figure 10 shows the variation of this activation energy barrier with loading, temperature, and time. It can be clearly seen from Figure 10 that setting $n = 2$ results in the overestimation of the energy barrier with respect to that predicted with the time-dependent n. Moreover, at low loadings, it is clear that the initial temperature effect (at $t = 0$) on the energy barrier is negligible and that the most significant factor in determining the magnitude of this energy barrier is the amount adsorbed. However, at high loadings, the energy barrier estimated with the time-dependent n increases markedly with temperature. Another condition that shows a marked effect of temperature on the activation energy is the short-time behavior ($0 < t < 80$ s), which resembles a transient state of molecules being transmitted from one energy level to another after providing the initial activation energy barrier at $t = 0$.

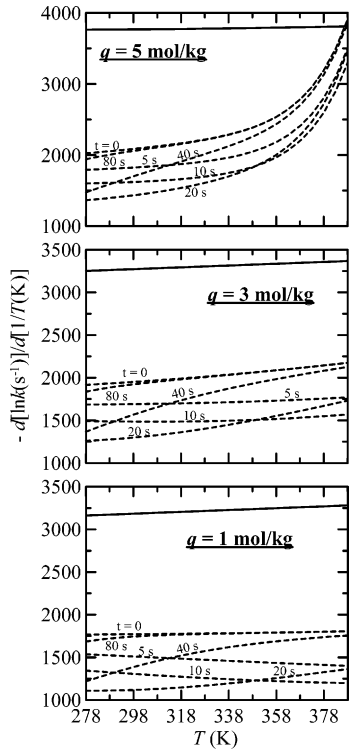

Figure 10. Effects of loading, temperature, and time on [∂ ln k (s^{-1})]/∂[1/T (K)] with loading predicted with second-order and time-dependent degrees of the parabolic concentration profiles (solid and dashed lines, respectively).

Figure 11 presents a demonstration of the correlations provided by the mass-transfer coefficients with $n = 2$ (given in Table 3) and with time-dependent n (given in Table 3 and eq 4) at various pressure steps. It can be seen that the correlated fractional uptakes with k' involving the time-dependent n are always more accurate than those based on $n = 2$. Moreover, it can be seen that this approach preserves its accuracy of correlating the fractional uptakes even at high pressures at which the measurements of the microbalance suffered from a minor noise due to the lower accuracy of the pressure transducer at those pressures. The predictability of the uptakes exhibited the same qualities at different temperatures. Nevertheless, at $T = 383$ K, the predicted uptakes did not estimate the measured fractional uptakes adequately with the ~3 Torr pressure step changes. However, they succeeded in predicting the

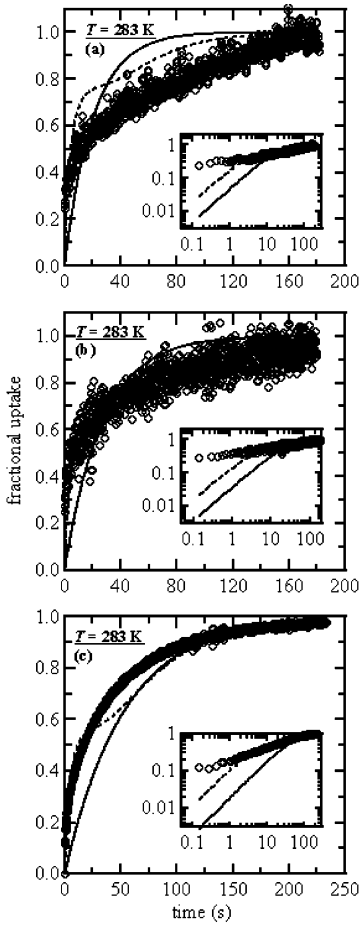

Figure 11. Experimental fractional uptakes (symbols) at 283 K and pressure steps of (a) 442−514, (b) 89−92, and (c) 2.6−5.5 Torr predicted with the LDF model and second-order and time-dependent concentration profiles (solid and dashed lines, respectively). The inserts show logarithmic-scale representations of the same surrounding figures.

fractional uptakes measured after the pressure step size was increased to ∼30 Torr. This artifact is attributed to the very low affinity for adsorption at very high temperatures.

Conclusions

The dynamic uptakes of *n*-butane on BAX-1100 activated carbon were measured gravimetrically using an automated VTI microbalance in the temperature and pressure ranges of 283−383 K and ∼3−1000 Torr, respectively. The measurements were conducted with variable pressure step sizes to examine the effects of different amounts of heat evolved upon adsorption. A regression of the overall linear driving force (LDF) mass-transfer coefficients indicated that this latter effect was negligible on their magnitudes.

A stepwise analysis of the significant dependences of the overall mass-transfer coefficients on the operating conditions revealed that the most dominant factor is the Arrhenius dependence, which indicates an energy-activated adsorption mechanism, such as surface diffusion. However, it was found that the complete description of the Arrhenius character of diffusion requires the inclusion of the variations of the concentration profiles inside the particle with different operating conditions, namely, temperature. The amounts adsorbed resulted in a positive effect on the overall mass-transfer coefficients, especially at very low and very high loadings. Overall, a satisfactory representation of the experimental data was provided with the optimized mass-transfer coefficients.

The initial activation energy barrier for diffusion was found to be mostly independent of temperature, except at very high loadings. This behavior can be used as an indicator of the appearance of different interaction forces under the different dynamic conditions. Nevertheless, an apparent diffusion energy barrier was indicated at short times of diffusion. This apparent transient energy barrier is lower (in absolute value) than the initial energy barrier, but the difference between the two energy barriers diminishes at long times. The temperature effect on this apparent energy barrier becomes significant only under those transient conditions. The effects of loading were more pronounced than those of temperature, thereby resulting in an increase of the required activation energies.

Acknowledgment

The authors gratefully acknowledge financial support from the National Science Foundation under Grant CTS-9500362, MeadWestvaco, and the Separations Research Program at the University of Texas at Austin. Karen D. Daniel is also acknowledged for carrying out the experimental measurements of the uptake curves.

Literature Cited

(1) Ruthven, D. M. *Principles of Adsorption and Adsorption Processes*; John Wiley & Sons: New York, 1984.

(2) Do, D. D. *Adsorption Analysis: Equilibria and Kinetics*; Imperial College Press: London, 1998.

(3) Riekert, L. The Relative Contribution of Pore Volume Diffusion and Surface Diffusion to Mass Transfer in Capillaries and Porous Media. *AIChE J.* **1985**, *31*, 863.

(4) Kapoor, A.; Ritter, J. A.; Yang, R. T. On the Dubinin−Radushkevich Equation for Adsorption in Microporous Solids in the Henry's Law Region, *Langmuir* **1989**, *5*, 1118.

(5) Kapoor, A.; Yang, R. T. Contribution of Concentration-Dependent Surface Diffusion to Rate of Adsorption. *Chem. Eng. Sci.* **1991**, *46*, 1995.

(6) Weaver, J. A.; Metzner, A. B. The Surface Transport of Adsorbed Molecules. *AIChE J.* **1966**, *12*, 655.

(7) King, D. A. Surface Diffusion of Adsorbed Species: A Review. *J. Vac. Sci. Technol.* **1980**, *17*, 241.

(8) Garg, D. R.; Ruthven, D. M. The Effect of Concentration Dependence of Diffusivity on Zeolitic Sorption Curves. *Chem. Eng. Sci.* **1972**, *27*, 417.

(9) Yang, R. T.; Fenn, J. B.; Haller, G. L. Modification to the Higashi Model for Surface Diffusion. *AIChE J.* **1973**, *19*, 1052.

(10) Gilliland, E. R.; Baddour, R. F.; Perkinson, G. P.; Sladek, K. J. Diffusion on Surfaces. Effect of Concentration on the Diffusivity of Physically Adsorbed Gases, I. *Ind. Eng. Chem. Fundam.* **1974**, *13*, 95.

(11) Suzuki, M.; Fujii, T. Concentration Dependence of Surface Diffusion Coefficients of Propionic Acid in Activated Carbon Particles. *AIChE J.* **1982**, *28*, 380.

(12) Seidel, A.; Carl, P. S. The Concentration Dependence of Surface Diffusion for Adsorption on Energetically Heterogeneous Adsorbents. *Chem. Eng. Sci.* **1989**, *44*, 189.

(13) Arena, M. V.; Deckert, A. A.; George, S. M. Coverage-Dependent Surface Diffusion Expected from Multiple-Site Hopping Model. *Surf. Sci.* **1991**, *241*, 369.

(14) Hu, X.; Do, D. D.; Rao, G. N. Experimental Concentration Dependence of Surface Diffusion of Hydrocarbons in Activated Carbon. *Chem. Eng. Sci.* **1994**, *49*, 2145.

(15) Ruthven, D. M. Honorary Presentation on the Advances in Adsorption Science and Technology. Presented at the AIChE Annual Meeting, Los Angeles, CA, Nov 12−17, 2000.

(16) Ruthven, D. M. Measurement of Diffusion in Microporous Solids. In *Separation Technology*; Vansant, E. F., Ed.; Elsevier Science: New York, 1994; pp 1−26.

(17) Li, Z.; Yang, R. T. Concentration Profile for Linear Driving Force Model for Diffusion in a Particle. *AIChE J*. **1999**, *45*, 196.

(18) Sircar, S.; Hufton, J. R. Intraparticle Adsorbate Concentration Profile for Linear Driving Force Approximation. *AIChE J*. **2000**, *46*, 659.

(19) Sircar, S.; Hufton, J. R. Why Does the Linear Driving Force Model for Adsorption Kinetics Work? *Adsorption* **2000**, *6*, 137−147.

(20) Yang, R. T. *Gas Separation by Adsorption Processes*; Imperial College Press: London, 1997.

(21) Hsuen, H. K. An improved linear driving force approximation for intraparticle adsorption. *Chem. Eng. Sci.* **2000**, *55*, 3475.

(22) Nakao, S.; Suzuki, M. Mass Transfer Coefficient in Cyclic Adsorption and Desorption. *J. Chem. Eng. Jpn.* **1983**, *16*, 114.

(23) Buzanowski, M. A.; Yang, R. T. Extended linear driving-force approximation for intraparticle diffusion rate including short times. *Chem. Eng. Sci.* **1989**, *44*, 2683

(24) Liaw, C. H.; Wang, J. S. P.; Greenkorn, R. H.; Chao, K. C. Kinetics of fixed-bed adsorption: A new solution. *AIChE J*. **1979**, *54*, 376.

(25) Zhang, R.; Ritter, J. A. New Approximate Model for Nonlinear Adsorption and Diffusion in a Single Particle. *Chem. Eng. Sci*. **1997**, *52*, 3161.

(26) Botte, G. G.; Zhang, R.; Ritter, J. A. On the Use of Different Parabolic Concentration Profiles for Nonlinear Adsorption and Diffusion in a Single Particle. *Chem. Eng. Sci.* **1998**, *53*, 4135.

(27) Gadre, S. A.; Ritter, J. A. New analytical solution for nonlinear adsorption and diffusion in a single particle. *Chem. Eng. Sci.* **2002**, *57*, 1197.

(28) Georgiou, A; Kupiec, K. Nonlinear driving force approximation for intraparticle mass transfer in adsorption processes Nonlinear isotherm systems with macropore diffusion control. *Chem. Eng. J*. **2003**, *92*, 185.

(29) Choong, T. S. Y.; Scott, D. M. The Linear Driving Force Model for Cyclic Adsorption and Desorption: The Effect of External Fluid−Film Mass Transfer. *Chem. Eng. Sci*. **1998**, *53*, 847.

(30) Ritter, J. A.; Al-Muhtaseb, S. A.; McIntyre, J. A. Non-Equilibrium Adsorption Dynamics, and Their Role in the Modeling of PSA Process Behavior. In *Fundamentals of Adsorption 7*; Kaneko, K., Kanoh, H., Hanzawa, Y., Eds.; IK International, Ltd.: Chiba City, Japan, 2002.

(31) Liu, Y. J.; Holland, C. E.; Ritter, J. A. Solvent Vapor Recovery by Pressure Swing Adsorption. III. Comparison of Simulation with Experiment for the Butane-Activated Carbon System. *Sep. Sci. Technol.* **1999**, *34*, 1545.

(32) Al-Muhtaseb, S. A.; Holland, C. E.; Ritter, J. A. Adsorption of C_1 to C_7 Normal Alkanes on BAX Activated Carbon: 2. Statistically Optimized Approach for Deriving Thermodynamic Properties from the Adsorption Isotherm. *Ind. Eng. Chem. Res.* **2001**, *40*, 319.

Received for review May 5, 2004
Revised manuscript received August 2, 2004
Accepted August 11, 2004

IE049629R